Applied Catalysis B: Environmental 92 (2009) 126–137

Contents lists available at ScienceDirect

Applied Catalysis B: Environmental

journal homepage: www.elsevier.com/locate/apcatb

Effect of NO_x adsorption/desorption over ceria-zirconia catalysts on the catalytic combustion of model soot

I. Atribak [a], B. Azambre [b], A. Bueno López [a,*], A. García-García [a]

[a] Department of Inorganic Chemistry, University of Alicante, Ap. 99 E-03080, Alicante, Spain
[b] Université Paul Verlaine de Metz, LCME, Rue Victor Demange, 57500 Saint Avold, France

ARTICLE INFO

Article history:
Received 29 April 2009
Received in revised form 10 July 2009
Accepted 20 July 2009
Available online 25 July 2009

Keywords:
Catalyzed soot oxidation
Ceria
Ceria-zirconia mixed oxides
Soot
NO_x
Diesel
DRIFTS

ABSTRACT

CeO_2, ZrO_2 and $Ce_xZr_{1-x}O_2$ mixed oxides with different Ce/Zr ratios were prepared by (co-)precipitation and 500 °C-calcination, and were characterized by Raman spectroscopy, XRD and N_2 adsorption at −196 °C. The catalytic activity of these materials for soot oxidation by NO_x/O_2 has been correlated with the catalytic activity for NO_2 production, and the surface processes occurring upon $NO + O_2$ interaction with the different catalysts have been studied by *in situ* DRIFTS and NO_x adsorption and further He-TPD. The catalytic activity for soot combustion of cerium-containing catalysts depends on the NO_2 production capacity, and a linear relationship between the temperature of maximum NO_2 production and the temperature of half soot conversion has been obtained. In a first step, surface nitrites are formed upon catalysts interaction with $NO + O_2$, for all the catalysts. These nitrites are progressively converted to nitrates, and NO_2 is yielded after these adsorption/oxidation/desorption processes. For $Ce_xZr_{1-x}O_2$ mixed oxides, the catalytic activity for NO_2 production depends on the cerium content, the higher the better, rather than on the BET area of the catalyst. The whole results demonstrate that the production of NO_2 in the range of temperatures relevant to soot oxidation not only depends on the NO/nitrites oxidation capacity of the catalyst used but also probably on the adsorption strength of the nitrates under NO oxidation conditions. The thermostability of the nitrates adsorbed on zirconium sites is higher than that of nitrates adsorbed on cerium sites.

1. Introduction

Soot removal in Diesel exhausts is a topic of ongoing research due to the environmental and health impact of these carbon nanoparticles [1–5]. In the absence of NO_x, active oxygen yielded by ceria catalysts is able to perform soot oxidation [6] and surface oxygen may increase the soot oxidation rate by Mars and Van Krevelen spillover mechanism [7]. On the other hand, it is well known that NO_2 is much more oxidizing than NO and O_2 are [8]. Ceria-based materials are effective for the regeneration of soot traps, where the soot–catalyst contact is loose and the gas stream contains $NO + O_2$, because they oxidize NO to NO_2 efficiently. This reaction pathway allows fast soot oxidation even under loose contact of soot and catalyst. For ceria, the maximum of NO oxidation to NO_2 is observed around 450 °C, and above this temperature, the NO conversion is limited thermodynamically [9]. The elementary steps of NO oxidation are thought to involve either Langmuir–Hinshelwood or Eley–Rideal mechanisms, which can be depicted by the following reactions:

$$NO\,(\text{gas or adsorbed}) + O* \rightarrow NO_2 + \square \quad (1)$$

$$O_2 + 2\square \rightarrow 2O* \quad (2)$$

In this mechanism, □ denotes an oxygen vacancy and O* an active oxygen on ceria.

It has been reported [10–12] that the catalytic activity for soot combustion of CeO_2 can be significantly improved by Zr^{4+} doping. This improvement has a minor effect for catalysts calcined at 500 °C, but the Ce-Zr mixed oxides present enhanced thermal stability in comparison to pure CeO_2, maintaining part of its activity for soot oxidation and selectivity towards CO_2 formation after calcination at temperatures as high as 1000 °C [11,12]. CeO_2 doping with some other rare-earth metal cations, such as La^{3+} or $Pr^{3+/4+}$, also enhances the thermal stability of CeO_2, and the Ce-La and Ce-Pr mixed oxides also present increased catalytic activity with regard to bare ceria after thermal deactivation [6,13–15]. Thermal stability is a mandatory requirement for a soot oxidation catalyst, since the temperature inside a Diesel Particulate Filter (DPF) can increase up to 1000–1100 °C as a consequence of the highly exothermal soot combustion process, with temperature gradients of 100 °C/cm along both radial and longitudinal directions of the DPF [16].

* Corresponding author. Tel.: +34 965903400x2226; fax: +34 965903454.
E-mail address: agus@ua.es (A. Bueno López).

0926-3373/$ – see front matter © 2009 Elsevier B.V. All rights reserved.
doi:10.1016/j.apcatb.2009.07.015

The catalytic activity of ceria catalysts, including both pure and mixed oxides, for soot oxidation by NO_x/O_2 depends on their textural properties (BET area; crystallite size), but other properties of the oxides, such as their redox behavior and/or lattice oxygen mobility, can also play a significant role [12,14,15].

In spite of the promising activity of Ce-Zr mixed oxides for soot combustion [5,10–12], the information available about the soot combustion mechanism under NO_x/O_2 gas streams is limited. This is because most articles focussed on the study of this mechanism have been carried out with pure ceria or with ceria doped with cations different to Zr^{4+} [5,6,8,9,12,14,15]. Thus, the goal of the current study is to investigate the adsorption/desorption of NO_x on ceria and ceria-zirconia catalysts, and to analyze the participation of these key steps in the catalyzed oxidation of NO to NO_2. The catalytic activity of these materials for soot oxidation is correlated with the catalytic activity for NO_2 production, and the surface processes occurring upon $NO + O_2$ interaction (among other atmospheres) with the different catalysts are discussed.

2. Experimental

2.1. Catalyst preparation

CeO_2, ZrO_2 and $Ce_xZr_{1-x}O_2$ mixed oxides with different metal ratio were prepared using a (co-)precipitation route. The required amounts of $ZrO(NO_3)_2{\cdot}nH_2O$ and/or $Ce(NO_3)_3{\cdot}6H_2O$ (supplied by Aldrich) were dissolved in water and the hydroxides were precipitated by dropping an ammonia solution to keep the pH about 9. The precipitates were dried at 90 °C overnight and calcined in air for 3 h at 500 °C.

2.2. Catalyst characterization

The catalysts were characterized by N_2 adsorption at −196 °C in an automatic volumetric system (Autosorb-6B from Quantachrome) after degassing the samples at 250 °C for 4 h.

Raman spectra were recorded in a LabRam Jobin-Yvon (Horiba) spectrograph coupled to a microscope. He/Ne laser (λ = 632.82 nm) source was used as source of light and a Perltier cooled CCd as detector. A power of approximately 0.9 mW reached the sample through a ×50 VLWD (n/a = 0.50) objective for 3 s and 15 consecutive spectra were added to obtain the final spectrum.

X-ray diffractograms were measured on a Seifert powder diffractometer using the CuKα radiation (λ = 0.15418 nm). Spectra were recorded between 10° and 60° (2θ) with a step size of 0.05 and measuring for 3 s at each step.

2.3. Catalytic tests

Catalytic tests were performed in a fixed-bed reactor under a 500 ppm NO_x + 5%O_2 gas flow (500 ml/min; GHSV 30000 h^{-1}). The model soot used was a carbon black from Degussa (Printex-U). The experiments consisted of heating the soot–catalyst mixtures from 25 to 750 °C at 10 °C/min. The soot–catalyst mixtures contained 80 mg of catalyst + 20 mg of soot + 300 mg SiC, and were prepared with a spatula following the so-called "loose contact" procedure. The gas composition was continuously monitored by specific NDIR-UV gas analyzers for NO, NO_2, CO, CO_2 and O_2, and the measurement data are recorded every 30 s. Blank experiments were performed with catalysts (without soot).

2.4. DRIFTS in situ

Diffuse reflectance spectra were recorded in the 4000–700 cm^{-1} range (resolution 4 cm^{-1}, 100 scans) on a Varian Excalibur 4100HE spectrometer equipped with a MCT detector and a Graseby Specac "The Selector" DRIFTS optical accessory. Pure catalysts (without diluents) were loaded into a Spectra-Tech environmental cell designed to work up to 500 °C under controlled temperature and flowing gases. Prior to adsorption, all the catalysts (previously calcined in air at 500 °C) were thermally treated *in situ* at 380 °C under He. Time-resolved spectra obtained during the exposure of the different catalysts to NO (2000 ppm/He), NO_2 (2000 ppm/He) or $NO + O_2$ (2000 ppm + 5%) at 30 or 350 °C were recorded in single-beam (SB) mode. Then pseudo-absorbance spectra were re-calculated using the SB spectrum of the fresh catalyst prior to adsorption as background. Semi-quantitative measurements of the populations of the different ad-NO_x species were performed using the Resolutions Pro v. 4.1.0. software.

2.5. Temperature programmed desorption (TPD) experiments

The adsorption/desorption of NO_x on CeO_2, $Ce_{0.76}Zr_{0.24}O_2$ and ZrO_2 were investigated by temperature programmed desorption experiments under He after NO_x adsorption at 60 or 350 °C.

2.5.1. Adsorption at 60 °C + He-TPD

The catalysts were outgassed at 130 °C under high vacuum to clean the surface and then were exposed to the selected reactive gas (2000 ppm NO/5%O_2/He balance or 2000 ppm NO_2/He balance) at 60 °C during 12 h into a home-made adsorption chamber. Then, 20 mg of catalyst was placed inside a quartz tube coupled to a HP 5973 mass detector working in electron impact (EI) mode at 70 eV, and heated from 25 up to 700 °C at a heating rate of 10 °C/min using He as the carrier gas. Individual desorption profiles of NO, NO_2 and O_2 were calculated from their known relative contributions to fragments m/z = 28, 30, 32, and 46 a.m.u. and subsequent normalization.

2.5.2. Adsorption at 350 °C + He-TPD

The catalytic test bench was constituted by a fixed-bed reactor coupled to a Biorad FTS185 infrared spectrometer and equipped with a FTIR gas cell (path length = 2 m) and MCT detector. 200 mg of catalyst was exposed for 1 h to a 70 ml/min gas flow with 2000 ppm NO/5%O_2/He balance. Then, this gas mixture was replaced by pure He and the catalyst was maintained for 1 h at 350 °C under the inert gas for weakly bound NO_x species removal. Finally, a TPD was performed raising the temperature from 350 to 600 °C at 10 °C/min.

3. Results and discussion

3.1. Catalysts characterization

The Raman spectra of the catalysts are included in Fig. 1. CeO_2 presents the F_{2g} vibration mode of the fluorite (cubic) type lattice at 463.5 cm^{-1}.

The Raman spectrum of ZrO_2 presents features of both monoclinic and tetragonal zirconia phases. Pure tetragonal zirconia presents six Raman-active modes of $A_{1g} + 3E_g + 2B_{1g}$ symmetry (space group $P4_2/nmc$). For the ZrO_2 sample, these six bands are observed at 148, 267, 322, 464, 610 and 648 cm^{-1}. Monoclinic zirconia presents 18 Raman-active modes. Some of these bands are clearly observed in the ZrO_2 spectrum, such as the doublets at 180–190 and 539–559 cm^{-1} and single bands at 333, 380, 475, 502, 618 and 757 cm^{-1} [17]. However, some of the mentioned bands are not resolved in Fig. 1 and some monoclinic and tetragonal bands overlap. Considering the intensities of the bands observed in Fig. 1, monoclinic zirconia is the most abundant phase of the ZrO_2 catalyst, and is also the thermodynamically stable phase at ambient conditions. Nevertheless, the tetragonal

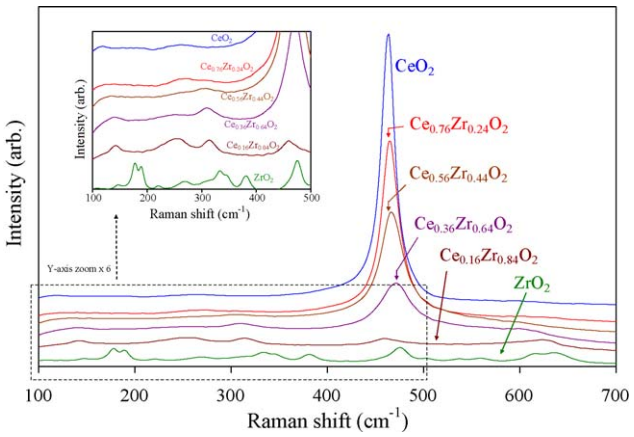

Fig. 1. Raman characterization of catalysts.

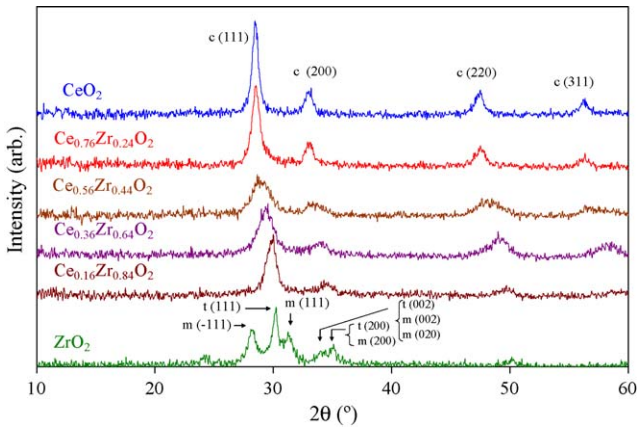

Fig. 2. XRD characterization of catalysts (c: cubic; t: tetragonal; m: monoclinic).

phase can be favored over the monoclinic one below a critical crystallite size [18].

The Raman spectrum of the catalyst $Ce_{0.16}Zr_{0.84}O_2$ contains five of the six bands attributed to the tetragonal phase of zirconia, whose Raman shifts, however, appear at lower values (140, 250, 313, 458, 590 and 622 cm^{-1}) [18]. Besides, it is described in the literature that the bands at 610 and 640 cm^{-1} shift and overlap for mixed oxides of composition close to $Ce_{0.2}Zr_{0.8}O_2$ [19]. Therefore, the assignment for this catalyst would be t-$Ce_{0.16}Zr_{0.84}O_2$ mixed oxide.

For the other mixed oxides, a progressive shift of the strong fluorite band from 463.5 to 473.0 cm^{-1} occurs as the cerium loading decreases from $x = 1$ to $x = 0.36$. This shift has been attributed to the cell contraction due to zirconium incorporation into the ceria lattice [20]. The Raman spectra of the fluorite-type oxide structures are dominated by oxygen lattice vibrations and Zr doping affects this vibration leading to the decrease of the band intensity. This Raman characterization suggests the progressive shift of the $Ce_xZr_{1-x}O_2$ structure from cubic to tetragonal as the cerium loading decreases from $x = 1$ to $x = 0.16$. The same trend has been reported for commercial $Ce_xZr_{1-x}O_2$ samples synthesized by Rhodia using a precipitation route from nitrate precursors [21]. It was published that the commercial samples with molar cerium content higher than 68% exhibited a cubic structure whereas a tetragonal structure was evidenced for mixed oxides with lower cerium content (50% and 15%). On the contrary, the structure of the pure zirconia sample was monoclinic [21].

The catalysts $Ce_{0.36}Zr_{0.64}O_2$ and $Ce_{0.56}Zr_{0.44}O_2$ also show the bands at 140, 250 and 313 cm^{-1} of the tetragonal $Ce_{0.16}Zr_{0.84}O_2$ mixed oxide. The intensity of these three bands decreases as the zirconium loading decreases, and they are not observed in the spectra of $Ce_{0.76}Zr_{0.24}O_2$. The presence of these very weak features can be compatible with t′/t″ structures [22–24], but the contribution of f–f transitions due to lanthanides impurities cannot be excluded [25].

The XRD patterns of the catalysts are included in Fig. 2, and the conclusions reached by Raman are confirmed by this technique. CeO_2 presents the reflections typical of the fluorite structure at 28.5°, 33.1°, 47.6°, 56.5°, and 59.2°, corresponding to the (1 1 1), (2 0 0), (2 2 0), (3 1 1) and (2 2 2) planes [26]. The XRD pattern of the catalyst ZrO_2 contains the main reflections of the monoclinic ((−1 1 1) and (1 1 1) at 28.2° and 31.4°, respectively) and tetragonal ((1 1 1) at 30.2°) phases, in agreement with the Raman results. The catalyst $Ce_{0.76}Zr_{0.24}O_2$ clearly presents cubic structure, which is supported by the fact that the position of their peaks is the same to that of CeO_2 peaks. The Scherrer's equation predicts crystallite sizes of 14 and 11 nm for CeO_2 and $Ce_{0.76}Zr_{0.24}O_2$, respectively. On the other hand, the catalyst $Ce_{0.16}Zr_{0.84}O_2$ mainly presents tetragonal structure, as deduced from the position of the main peak at 30°, which is that expected for the tetragonal (1 1 1) plane. In addition, the low intensity broad band at 34.7° can be attributed to the tetragonal contributions (0 0 2) and (2 0 0). The diffractograms of the catalysts with intermediate zirconium content ($Ce_{0.36}Zr_{0.64}O_2$ and $Ce_{0.56}Zr_{0.44}O_2$) suggest a progressive tetragonalisation of the structure as the most intense peaks were shifted to higher diffraction angles by increasing the Zr content. This observation was attributed to shrinkage of lattice due to the replacement of Ce^{4+} by the smaller Zr^{4+} cation. The peak broadening and asymmetry observed mainly for $Ce_{0.56}Zr_{0.24}O_2$ catalyst could suggest the presence of both cubic and tetragonal reflexions. For instance, the peak around 29° seems to contain contribution of the cubic (1 1 1) and tetragonal (1 1 1) planes. For $Ce_xZr_{1-x}O_2$ catalysts with $x < 0.76$, the crystallite size cannot be estimated properly from XRD patterns since the tetragonal and cubic peaks overlapping could affect the peak broadening.

As a summary, the XRD results support the Raman conclusions about the progressive shift of the $Ce_xZr_{1-x}O_2$ structure from cubic to tetragonal as the cerium loading decreases from $x = 1$ to $x = 0.16$.

The BET surface areas of the catalysts are included in Table 1. Among the samples tested, the catalysts CeO_2, ZrO_2 and $Ce_{0.76}Zr_{0.24}O_2$ reach the highest areas (64–67 m^2/g), and $Ce_xZr_{1-x}O_2$ catalysts with lower zirconium loading present BET areas between 8 and 47 m^2/g. The lack of a clear trend of BET surface areas with the zirconium content could be attributed to the fact that each composition presents a different crystalline structure or even mixture of crystalline structures. A similar trend in BET area with the zirconium loading was reported [27] for a set of commercial $Ce_xZr_{1-x}O_2$ samples, but with higher absolute BET values. Among these commercial samples, the highest BET area was obtained with bare CeO_2 (284 m^2/g), and the surface area decreased as the Zr content increased, in agreement with our results. For this commercial set of samples, the lowest BET area was obtained with the formulation $Ce_{0.5}Zr_{0.5}O_2$ (87 m^2/g). The argument provided to explain such trend was that the zirconium addition facilitates crystallite growth of cerium oxide [27]. However, this growth takes place when zirconium content is

Table 1
Catalyst characterization by N_2 adsorption at −196 °C.

Catalyst	BET (m^2/g)
CeO_2	64
$Ce_{0.76}Zr_{0.24}O_2$	67
$Ce_{0.56}Zr_{0.44}O_2$	31
$Ce_{0.36}Zr_{0.64}O_2$	8
$Ce_{0.16}Zr_{0.84}O_2$	47
ZrO_2	65

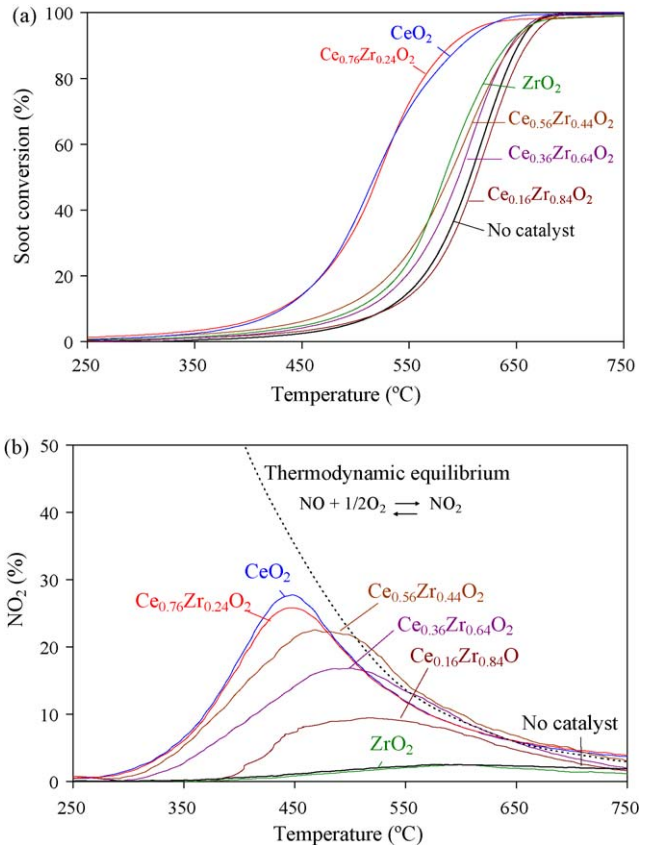

Fig. 3. Effect of the catalyst composition on the $Ce_xZr_{1-x}O_2$-catalyzed soot conversion (a) and NO_2 formation in blank experiments (without soot) (b).

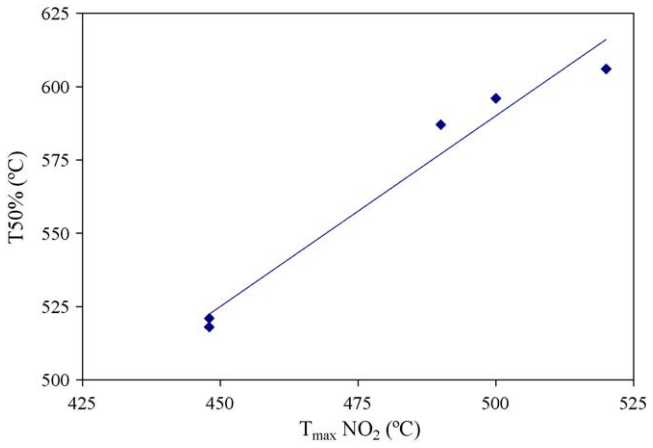

Fig. 4. Relationship between the catalytic activity of $Ce_xZr_{1-x}O_2$ for soot combustion and for NO oxidation to NO_2. T50% (°C): temperature for 50% soot conversion, obtained from Fig. 3a; $T_{max}NO_2$ (°C): temperature of maximum NO_2 concentration, obtained from Fig. 3b.

smaller than a certain loading ($x = 0.5$ for the commercial samples and $x = 0.36$ for samples prepared by co-precipitation in the current study). Above this critical value, ZrO_2 is responsible for the progressive change of the solid solution structure.

3.2. Catalytic tests

Soot conversion profiles are included in Fig. 3a and b compiles the NO_2 percentage measured in blank experiments (without soot). CeO_2 and $Ce_{0.76}Zr_{0.24}O_2$ show similar catalytic activity for soot combustion under the experimental conditions of these catalytic tests, and both catalysts present superior activity than catalysts with higher Zr content. In previous studies it was reported that $Ce_{0.76}Zr_{0.24}O_2$ is more resistant towards thermal deactivation than bare CeO_2 [10,12], thus being more convenient for a practical application. The catalytic activity of $Ce_xZr_{1-x}O_2$ samples with $x < 0.76$ is poor and the catalyzed soot combustion takes place in a range of temperature quite similar to that of the uncatalyzed reaction.

From blank experiments it is deduced that all the cerium-containing catalysts accelerate the oxidation of NO to NO_2 (Fig. 3b), in accordance with literature [12,27], while ZrO_2 does not present such behavior under the reaction conditions of these experiments (GHSV = 30000 h^{-1}). However, experiments performed with much lower GHSV (12000 h^{-1}) showed that ZrO_2 also presents a certain capacity to oxidize NO to NO_2.

As shown in Fig. 3b, $Ce_{0.76}Zr_{0.24}O_2$ and CeO_2 present the same NO_2 profile, with NO_2 formation above 275 °C and a maximum NO_2 level at 450 °C where the thermodynamic equilibrium of the NO oxidation reaction is reached. Above this maximum, the NO_2 level decreases following thermodynamics. The NO_2 production capacity decreases with the cerium loading, that is, the temperature of the maximum NO_2 production increases and the maximum NO_2 percentage reached decreases progressively as "x" decreases. Note that the inlet gas does not contain NO_2, but only NO + O_2, and in the absence of catalyst less than 3% of NO is oxidized to NO_2 because of the effect of temperature.

The relationship between catalytic activity for soot combustion and for NO_2 production has been analyzed in detail. In Fig. 4, the temperature required for 50% soot conversion (T50%) in catalytic tests has been plotted as a function of the temperature of maximum NO_2 production ($T_{max}NO_2$) in blank experiments. The results of all the experiments of Fig. 3 have been included in this plot, except that of ZrO_2 because its NO_2 production is equal to that measured with the empty reactor.

A linear relationship between the parameters "$T_{max}NO_2$" and "T50%" has been obtained (Fig. 4), which demonstrates that, as a general trend, the catalytic activity for soot combustion of a certain catalyst depends on its NO_2 production capacity. A relationship between $T_{max}NO_2$ and T50% was also obtained previously with a set of copper/alumina catalysts [28]. Taking into account these results, the catalytic combustion of soot under NO_x/O_2 is initiated by the attack of NO_2 to the soot surface, and once the soot surface is partially oxidized and the temperature is high enough, some other oxidizing species such as molecular O_2 or active oxygen atoms released by the ceria catalysts [29], are also able to oxidize soot along with NO_2.

For the ceria-zirconia mixed oxides prepared in the current study, their catalytic activity for NO oxidation to NO_2 mainly depends on their composition. This is deduced from Fig. 5a, where the parameter $T_{max}NO_2$ is plotted as a function of the cerium molar fraction. The data corresponding to bare CeO_2 is out of the trend followed by the mixed oxides, that is, the catalytic activity of this sample is lower than that expected considering its cerium content. This could be due to several factors. The first one, but probably not the most important, is the propensity of the mixed oxides in adsorbing CO_2, which is itself linked to their Lewis basicity. It is well known that CO_2 is an unavoidable contaminant of ceria and that the Lewis basicity of CeO_2 is higher than that of ZrO_2. By contrast, the relative Lewis basicity of the mixed oxides is not accurately known though $Ce_{0.69}Zr_{0.31}O_2$ was reported to be slightly more basic than $Ce_{0.21}Zr0_{.79}O_2$ and more than ZrO_2 [30]. In NO_x-TPD-MS experiments, which are discussed afterwards, and despite the outgassing under vacuum at 130 °C, a strong CO_2 desorption peak at temperature of about 400 °C was observed for almost all compositions. Hence, the rather basic character of ceria-zirconia

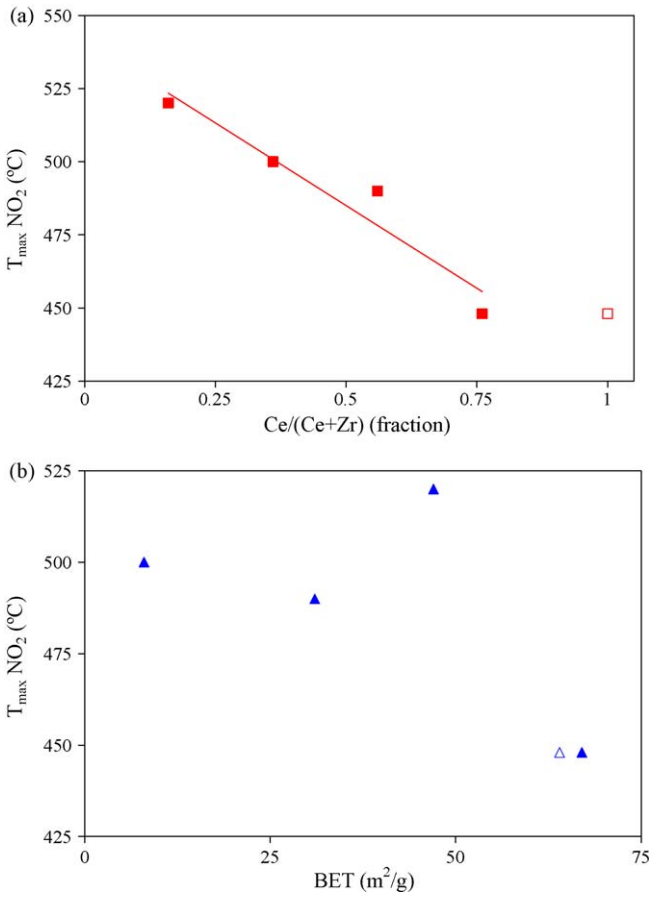

Fig. 5. Relationship between catalytic activity for NO oxidation to NO_2 ($T_{max}NO_2$) and cerium content (a) and BET surface area (b) of the cerium-containing catalysts. (Open symbols: bare ceria; solid symbols: Ce-Zr mixed oxides.)

solutions make them sensitive to poisoning by the CO_2 formed in soot combustion experiments or adsorbed from the atmosphere under storage conditions. CO_2 being a Lewis acid (like NO_2), it can react with basic oxygen sites to form rather stable surface or bulk carbonate-like complexes, which can inhibit partially the O* storage/release and/or NO_x oxidation/storage functions in the catalysts. The competition between CO_2 and NO_2 onto the same catalyst sites is expected during soot oxidation at moderate temperatures only (100–500 °C), where the effect of NO_x is also prominent. Due to the differences existing in their basicity, this competition should perhaps be more problematic for CeO_2 than for the mixed oxides. This will be investigated in a further study.

The second point, and probably the most important, is the availability of the reactive oxygens needed for the oxidation of NO. In the literature, it has been reported that mixed oxides with x = 0.6–0.8 (x = cerium molar fraction) have usually the highest OSC and hence the highest activities in oxidation reactions. Recently, the enhancement of the OSC for these mixed oxides in comparison with CeO_2 has been explained on the existence for the former of distinct nanodomains differing slightly in their composition within the ceria-zirconia crystallite [31]. In this study, it was claimed that the most active O species responsible for OSC activity could be located at the interfacial area between compositional nanopatches enriched either in Ce or Zr. In another study using FTIR of O_2 adsorption [32], it has been reported that the concentration of superoxide O_2^- species resulting from O_2 activation (on one-electron defect vacancies) also reached a maximum for samples having the highest OSC. Though the relative concentration of the activated O* species could not be easily monitored in our case, it is reasonable to think that the maximum of NO_2 production capacity observed for x = 0.6–0.8, as shown on Figs. 3–5, could also be correlated to the intrinsic ability of the catalysts in forming these superoxide species.

On the other hand, the BET surface area of the ceria-zirconia samples tested in the current study plays a minor role in the catalytic activity for NO oxidation to NO_2, and hence, in soot combustion catalytic activity. This is deduced from Fig. 5b, where scramble data are obtained in the plot of $T_{max}NO_2$ against BET area of the catalysts. Some authors have reported the dependence of the activity of cerium oxide-based catalysts with the BET area. For instance, a relationship between catalytic activity for soot oxidation with oxygen and BET area of the catalyst (soot and catalyst in tight contact) was reported for 5% iron-doped ceria samples calcined at different temperatures [11], and the same conclusion has been reported for catalysts with formulation $CeREO_2$ (RE = 10 wt.% of Pr, La, Sm or Y) calcined at 1000 °C [13]. In a previous study [12], we also obtained a relationship between catalytic activity for soot oxidation under NO_x/O_2 and BET area of $Ce_{0.76}Zr_{0.24}O_2$, for samples calcined at various temperatures within the range 500–1000 °C, that is, samples with equal composition but different area, and the same was observed for a set of CeO_2 catalysts [12]. According to these observations, it can be suggested that the catalytic activity for soot oxidation of ceria-based mixed oxides correlates well with the BET area of the samples if the cerium content of the samples compared is similar. However, if samples with very different cerium content are compared, the effect of nanoheterogeneity linked to a high cerium content seems to prevail. In order to reconcile the different viewpoints, it could be outlined that the concentration of the most active forms of oxygen is both function of the cerium content and the specific surface area. Higher surface densities (O^*/nm^2) are obtained for x = 0.6–0.8, but the specific surface area of CeO_2 is usually higher than the mixed oxides, which compensates its relatively lower surface concentration in anionic surface defects. The type of structure is important in terms of oxygen atoms diffusion from the bulk to surface and reversely.

Finally, in order to understand the NO_x–catalyst interactions that lead to the NO_2 production, and at the end, to the catalyzed soot combustion, the NO_x removal profiles obtained during the soot combustion and blank experiments were analyzed in detail. Some of these profiles were discussed elsewhere [12]. Unfortunately, under the experimental conditions of these experiments, the NO_x removal percentages are below 15% with all the catalysts tested. Hence, the effect of the catalyst composition on the NO_x–catalyst interactions cannot be properly interpreted. In order to get insight into such interactions, *in situ* DRIFTS characterization was performed and specific adsorption + TPD experiments were designed. The results obtained following both approaches are presented and discussed in the coming sections.

3.3. DRIFTS in situ

The structure and conditions of formation of ad-NO_x species was studied by IR spectroscopy (*in situ* DRIFTS). The time-dependence of the main ad-NO_x species (nitrites and nitrates) was determined by exploiting the IR spectra semi-quantitatively. Though semi-quantitative DRIFTS data cannot be considered as a direct measurement of the populations related to any peculiar ad-NO_x species, they were found useful to assess the effects of the reactive gas (NO, NO_2, NO + O_2) and temperature (30 or 350 °C) as well as those related to the composition of the ceria-zirconia catalysts.

3.3.1. Effect of reaction conditions on NO_x adsorption over $Ce_{0.76}Zr_{0.24}O_2$

First, the interaction of different gas mixtures (NO, NO + O_2 and NO_2) with the catalyst $Ce_{0.76}Zr_{0.24}O_2$ at different temperatures is discussed.

Time-resolved spectra and the corresponding semi-quantitative evolution of some adsorbed intermediates identified upon NO + O_2 interaction with $Ce_{0.76}Zr_{0.24}O$ at 30 °C are shown on Figs. 6a and 7a–c, respectively. In the early stages of this reaction (Fig. 6a), the main feature is the formation of a single broad band at 1180 cm^{-1}, which grows with time up to 10–15 min and then decreases in intensity. Due to the absence of any mode corresponding to N=O, this band can be assigned either to the nitrosyl anion NO^- (Eq. (3)) but more likely to chelated/bridged bidentate nitrites NO_2^- (Eq. (4)) [33,34]. The simultaneous negative absorption ca 3690 cm^{-1} (Fig. 7c) proves that some surface OH groups have reacted with NO.

$$NO + 2Ce^{4+}{-}OH^- \rightarrow Ce^{4+}{-}NO_2^- + Ce^{3+}{-}\square + H_2O \quad (3)$$

$$Ce^{3+}{-}\square + NO \rightarrow Ce^{4+}{-}NO^- \quad (4)$$

In these reactions, "Ce^{3+}–□" represents an oxygen vacancy linked to a Ce^{3+} cation and Ce^{4+}–OH^- an hydroxyl group on a Ce^{4+} cation. The Zr^{4+}–OH^- groups could also react with NO, like occurs in reaction (3), but OH on Ce^{4+} is expected to be more reactive than OH on Zr^{4+}.

In case that NO_2 is formed by NO oxidation, NO_2 could also yield nitrites (Eq. (5)). This process is not expected to be very important at 30 °C, since NO oxidation is kinetically restricted at low temperature, but could become important at higher temperature.

$$Ce^{3+}{-}\square + NO_2 \rightarrow Ce^{4+}{-}NO_2^- \quad (5)$$

Here, it has to be mentioned that the existence of anionic NO^- species, as suggested by Eq. (4) and in Ref. [35], cannot be proven by the present experimental data because their IR absorption were reported to closely match with those of chelated or bridged nitrites [34,36]. However, considering the strong oxidizing properties of ceria-based materials, it is possible that NO^- anions exist as transient species in the electron and/or oxygen transfer processes involved in the formation of nitrites from NO:

$$Ce^{4+}{-}NO^- + Ce^{4+}{-}O* \rightarrow Ce^{4+}{-}NO_2^- + Ce^{3+}{-}\square \quad (6)$$

where Ce^{4+}–O* is an active oxygen on ceria.

At higher reaction times, new absorption bands were found to grow together in the 1620–1450, 1300–1200 and 1050–1000 cm^{-1} regions (Fig. 6a, 65 min). According to the presence of strong overtones and combination modes in the 3300–2200 cm^{-1} region, the corresponding species are unambiguously ascribed to nitrates in a variety of structures/configurations ranging from bridged (1650–1600, 1225–1170 and 1030–1000 cm^{-1}) to bidentate (1565–1500, 1300–1260 and 1040–1010 cm^{-1}) and monodentate (1530–1480, 1290–1250 and 1035–970 cm^{-1}) NO_3^- species [34]. Since these absorptions grow at the expense of the 1180 cm^{-1} band (Figs. 6a, and 7a and b), one pathway leading to the formation of nitrates should be the oxidation of some bidentate nitrites by an activated O* surface species [35]:

$$Ce^{4+}{-}NO_2^- + Ce^{4+}{-}O* \rightarrow Ce^{4+}{-}NO_3^- + Ce^{3+}{-}\square \quad (7)$$

An alternative pathway leading to nitrates from reaction of ceria-zirconia with NO + O_2 require the participation of NO_2 gas

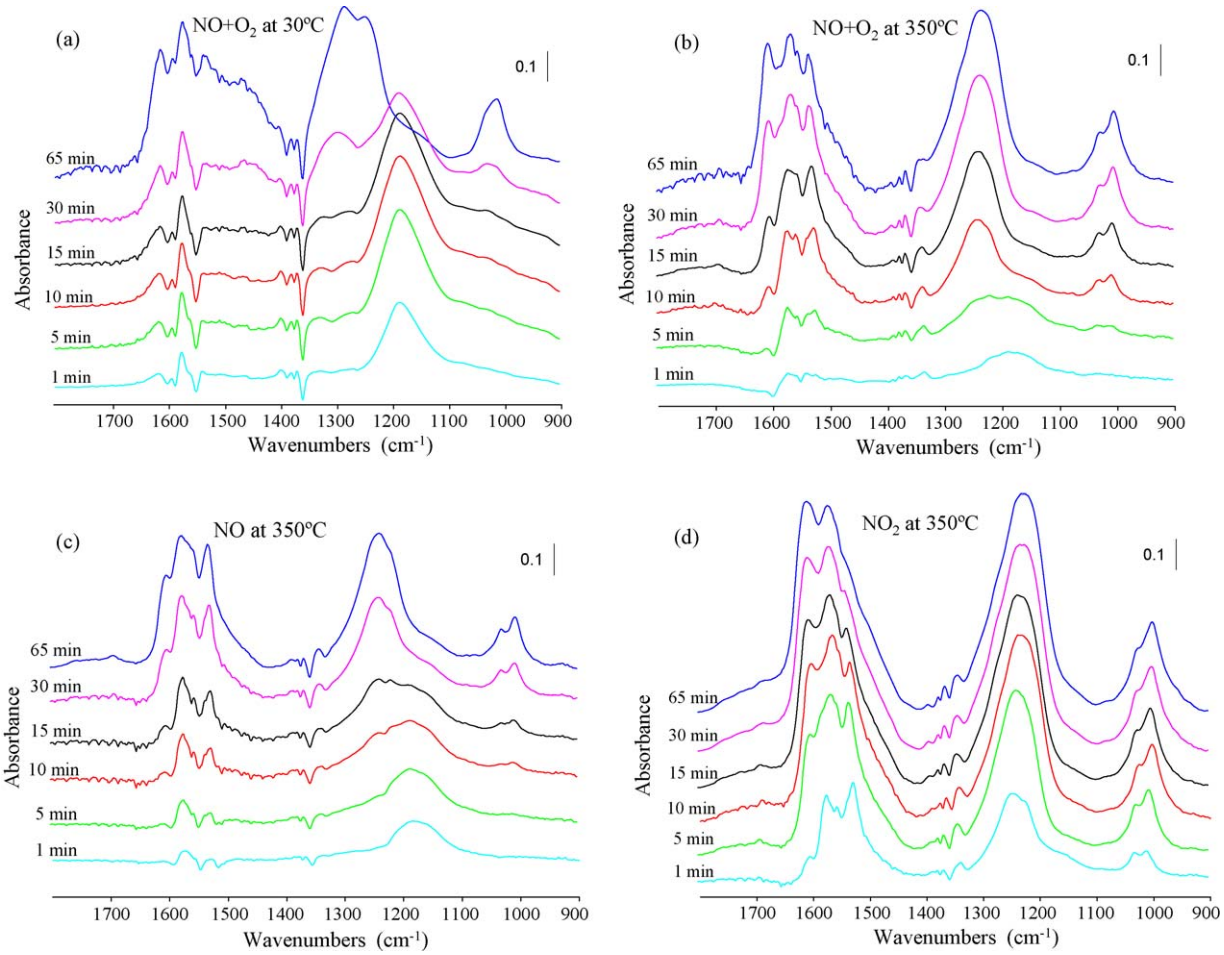

Fig. 6. Time-resolved DRIFTS spectra obtained with $Ce_{0.76}Zr_{0.24}O_2$ under different gas atmospheres and temperatures: (a) NO + O_2 at 30 °C, (b) NO + O_2 at 350 °C, (c) NO at 350 °C, and (d) NO_2 at 350 °C.

(formed via NO oxidation) as an intermediate (Eq. (8)). As shown on Fig. 7c, a consumption of surface OH groups, accompanied by the release of water, also occurs during the early minutes of reaction when the catalyst is exposed to NO_2 instead of $NO + O_2$.

$$NO_2 + 2Ce^{4+}{-}OH^- \rightarrow Ce^{4+}{-}NO_3^- + Ce^{3+}{-}\square + H_2O \quad (8)$$

A third reaction pathway that would also lead to the formation of surface nitrates, and does not require electron transfer from/to the catalyst surface, involves molecularly adsorbed NO_2 in the form of a N_2O_4 dimmer. In absence of adsorbed water, the self-disproportionation of the dimmer, which has been shown to occur on terrace sites of TiO_2 or defect-free MgO [34], is known to create a local pair of charged adsorbates formed by electron transfer from a NO_2 adsorbate to another and acid–base interaction with the surface:

$$2NO_2 \rightarrow N_2O_4 \rightarrow NO^+{-}NO_3^- \quad (9)$$

In presence of adsorbed water however, the NO^+ species are known to transform into NO_2^- species and new OH groups via the simultaneous release and reaction of protons with O surface sites [36].

In the present study, it is difficult to ascertain such kinds of mechanisms on ceria-zirconia, as the spectroscopic evidence for the existence of NO_x cationic species (such as NO^+ or NO_2^+) is not straightforward at any temperature (30 or 350 °C) and in presence/absence of O_2. In the literature, adsorbed NO_x^+ species were reported to absorb on metal oxides within a wide range of frequencies, typically between 2100 and 2390 cm^{-1} [34]. Here, some weak absorptions were observed ca 2220 and 1910 cm^{-1} (not shown on Fig. 6). They were also accompanied by a weak and ill-defined shoulder ca 1740 cm^{-1} possibly corresponding to adsorbed N_2O_4 [34]. All these bands were found to grow rather simultaneously to the nitrates at the later stages of adsorption and were also found in the experiments carried out at higher temperatures (350 °C). However, due to its position, the 1910 cm^{-1} band is better assigned to molecularly adsorbed NO on some M^{x+} cations or adsorbed N_2O_4 [34]. Moreover, the presence of the 2220 cm^{-1} band matches also rather well with the expected position of some combination mode of the nitrates compared with NO^+ [34]. Hence, we do not believe that stable cationic NO_x species exist on the ceria-zirconia surface under the conditions used in this study.

Finally, it must be mentioned that, for all the experiments carried out at 350 °C (Fig. 6b–d), the absorptions related to nitrates species tend to narrow in comparison to what was observed at ambient temperature (Fig. 6a). This is because of the decrease of the overall intensity in the 1500–1450 and 1300–1250 cm^{-1} regions, where the monodentate nitrates absorb. Indeed, this indicates that monodentate species become rather unstable on $Ce_{0.76}Zr_{0.24}O_2$ at 350 °C, yielding to a higher population of the bidentate and bridged forms. This seems in line with the known relative thermostabilities of the different kinds of nitrates.

Summarizing the IR data displayed on Fig. 6, it is clear that NO_x adsorption on ceria-zirconia at room temperature (Fig. 6a) and above (Fig. 6b–d) is reactive by nature and is dominated by electron and oxygen transfer processes. These processes create namely NO_x anionic species such as nitrites and nitrates. Before DRIFTS experiments, all the catalysts were pre-treated *in situ* under mild conditions (380 °C under He). During the pre-treatment, some partial dehydration/dehydroxylation as well as the decomposition of adsorbed C-containing species, such as CO_2-like species, occurred and these processes create some reduced sites on the surface. Another source for these sites however, as deduced from Eq. (3), could result from the reaction of NO with OH groups during the adsorption process. Among the possible locations of defective

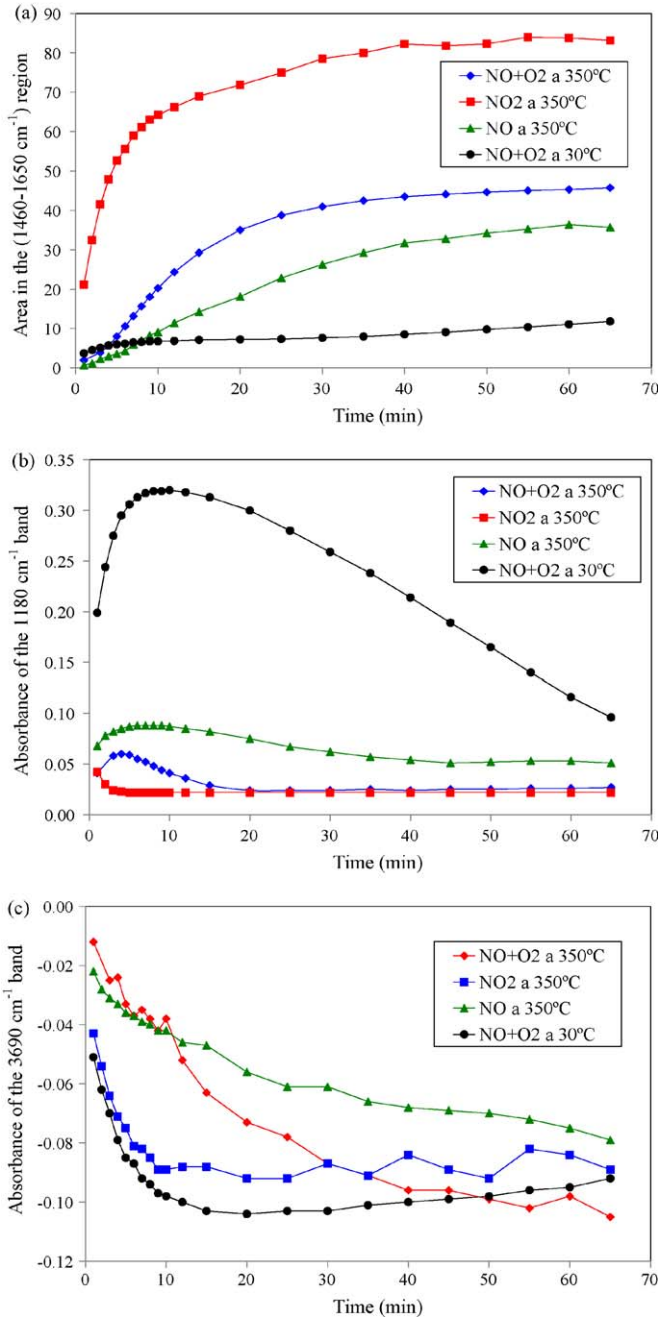

Fig. 7. Evolution of adsorbed intermediates estimated from DRIFTS spectra obtained with $Ce_{0.76}Zr_{0.24}O_2$ under different gas atmospheres and temperatures (spectra on Fig. 6). (a) Nitrates, (b) nitrites, and (c) hydroxyl groups.

sites, the most reactive ones are likely to be present on the side-terminations of the crystallites as well as on the interfaces between Ce- and Zr-enriched compositional nanodomains [31]. It is also worth noting that hyponitrites $N_2O_2^{2-}$ species were not detected on Fig. 6a, though they were already observed near room temperature by FTIR studies of NO_x adsorption on ceria-based surfaces [34,36]. In fact, the formation of such compounds requires the presence of two adjacent Ce^{3+}–□ reduced metal centres [36] and therefore a more complete reduction of the catalyst surface prior to adsorption.

When the $NO + O_2$ experiment was carried out at 350 °C (Fig. 6b), the same sequence observed at 30 °C (Fig. 6a) repeated. However, the oxidation of nitrites to nitrates (Eq. (7)) occurred at a much higher rate at 350 °C because the kinetic restrictions

observed at 30 °C do not apply. In fact, the activation barrier for electron transfer reactions is expected to be much smaller than the activation energy needed to break some M–O bonds to form new N–O bonds. The increased mobility/diffusion of the lattice oxygen from the bulk to the surface driven by the temperature can result in an enhanced rate for the surface oxidation of nitrites and also to an enhanced NO oxidation activity, yielding to more available NO_2. Both processes will promote the formation of nitrates as described before. In addition, the relative instability of surface nitrites at 350 °C on $Ce_{0.76}Zr_{0.24}O_2$ is well shown by comparing the relative amounts of these species at both temperatures on Fig. 7b.

The effect of gas-phase O_2 in the surface oxidation process can be assessed by comparing the DRIFTS data displayed on Fig. 6b and c. With NO alone (Figs. 6c, and 7a and b), the oxidation of nitrites still occurs, but obviously the rate of reaction is much slower than when O_2 is added along with NO to the feed. With NO alone, the reservoir of the O* species needed for the formation of nitrates from Eq. (7) is quickly depleted with no possibility to be replenished. In other words, it means that the diffusion of lattice oxygen may be still limiting at 350 °C. Hence, the question arises on the origin of the O* species involved in the enhancement of the oxidation processes in order to explain the results obtained in presence of O_2. The forms of O_2 activation on Ce-containing surfaces following dioxygen adsorption have been studied both by EPR [36], Raman [37] and FTIR [32]. These studies have shown that O_2 can be adsorbed following electron transfer by one-electron or two-electron surface defects as superoxide O_2^- or peroxide O_2^{2-}, respectively. Among these species, the surface superoxides are the most thermally unstable and convert first into peroxides as the temperature increases and then to lattice oxygen O^{2-} when the thermal activation is high enough to provide enough electron density to break the O–O bond. By comparing these experiments, it can be ensured that the active O* species needed for the oxidation of nitrites to nitrates arise firstly from the own oxygen reservoir on ceria samples (surface and/or lattice oxygen) and, eventually, from O_2 dissociation on oxygen vacancies following its adsorption as peroxide or superoxide [38].

As expected, the adsorption of NO_2 on $Ce_{0.76}Zr_{0.24}O_2$ (Fig. 6d) was found to strongly promote the formation of nitrates as their concentration reaches equilibrium after only 30 min at 350 °C in our conditions (Fig. 7a). In the case of NO_2, the population of nitrites formed initially was depleted already in the very early minutes of the reaction (Fig. 7b). Therefore, it means that NO_2 alone is very efficient in producing the active O* species to oxidize the nitrites in nitrates, such as:

$$Ce^{3+}{-}\square + NO_2 \rightarrow Ce^{4+}{-}O* + NO \quad (10)$$

This equation is in fact the reverse reaction depicted in Eq. (1) (NO oxidation) and will be only promoted in absence of O_2 from the gas phase. NO_2 being a strong oxidant, much more than O_2 and NO, one would also expect that the reoxidation of surface defects would occur at lower temperatures than with O_2.

3.3.2. Effect of ceria-zirconia composition on NO_x adsorption

The effect of the ceria-zirconia composition on the adsorption of NO + O_2 at 350 °C is discussed in this section. Whatever the peculiar composition/structure of the catalyst, the main ad-NO_x species detected at this temperature were bidentate nitrites and nitrates adopting namely the bidentate and bridged configurations. As was observed for $Ce_{0.76}Zr_{0.24}O_2$, the non-uniform distribution of the surface active sites and their various environments on the different ceria-zirconia resulted in a strong overlapping of bands related to nitrate species in the 1610–1500 and 1300–1200 cm^{-1} region of their IR spectra (not shown here), precluding their accurate assignment to any kind of site. As the surface coverage increases, discrete frequency shifts to higher wavenumbers were observed in the case of some bidentate nitrates. Usually, this phenomenon is explained by repulsive interactions existing between the adsorbate molecules when their local concentrations are high [34]. As a general rule for the compositions investigated, the band ca 1610–1600 cm^{-1} was also found to grow after the others, reflecting a lower reactivity of the site associated with this peculiar nitrate species. In order to address the effect of ceria-composition on NO_x adsorption more clearly, only the semi-quantitative DRIFTS data relevant to the formation of nitrites and nitrates as a whole are discussed here (Fig. 8). The formation of nitrates occurs at much higher rates for the intermediate and Ce-rich compositions (x = 1, 0.76, 0.56 and 0.36) than for the Zr-rich ones (x = 0 and 0.16). Note that this rate is slightly faster for $Ce_{0.76}Zr_{0.24}O_2$ and $Ce_{0.56}Zr_{0.44}O_2$ than for CeO_2, confirming that ceria doping by zirconia improves the oxidation capacity of the mixed oxide. Reversely, ZrO_2 was characterized by the highest amount of nitrites (and/or nitrosyl anion) and the lowest amount of nitrates over the time-scale investigated (65 min).

The trends observed in the formation rate of nitrates, i.e. oxidized ad-NO_x species, reflect somewhat the activities measured during NO oxidation tests (see Fig. 3b). As previously discussed, nitrates are promoted either when the amount of available NO_2 and/or the availability of reactive oxygen/hydroxyls are high. However, the relationship between NO oxidation activity (Fig. 3b) and ease of nitrates formation (Fig. 8) is not so straightforward. NO oxidation does not only depend on the intrinsic O mobility (O* delivery) of the mixed oxides but is also dependent on the relative surface coverage by the different ad-NO_x species, which may strongly vary from one oxide composition/structure to another as will be evidenced by TPD results presented below. This coverage-dependence enters in the kinetic limitations relevant to NO oxidation, which obviously apply mainly at low–medium temperatures. On the other hand, it is well known that the conversion of NO can also be limited at medium–high temperatures due to thermodynamics.

Finally, the participation of OH groups on the formation of ad-NO_x species, which was outlined in Eqs. (3) and (8), apparently increases with the Ce molar fraction (Fig. 8c). Therefore, this may show that the most reactive OH groups are linked to Ce atoms. Practically, these reactive OH groups are quickly depleted and this should in turn influence the surface processes with NO_x, resulting in the formation of new sorption sites.

3.4. NO_x adsorption + TPD experiments

3.4.1. He-TPD after NO + O_2 and NO_2 adsorption at 60 °C

TPD-MS profiles related to the desorption under He of adsorbed NO + O_2 and NO_2 at 60 °C on $Ce_xZr_{1-x}O_2$ are shown on Fig. 9a–c. The TPD data provided on Fig. 9 for NO_2, NO and O_2 (main gases observed) yield information about the relative strength and nature/amount of NO_x adsorption sites on the catalysts studied.

Though TPD is a powerful analytical tool complementary to DRIFTS to address the similitarities/differences existing among the $Ce_xZr_{1-x}O_2$ series, the following considerations have to be taken into account for a proper interpretation of the desorption profiles. First, the amount desorbed depends on the number of sites available for NO_x sorption. This number itself is a strong function of the specific surface area but also of the type of crystal planes exposed to the reactive gas. It has also to be mentioned that on all the samples investigated, a significant poisoning by carbonates was noticed, which manifests in TPD patterns by CO_2 peaks (m/z = 44 and m/z = 12) at ca 250 and 350–400 °C. CO_2 being a weak Lewis acid, it can compete with NO_2 onto the same adsorption sites in line with the rather basic character of ceria-zirconia. Second, the

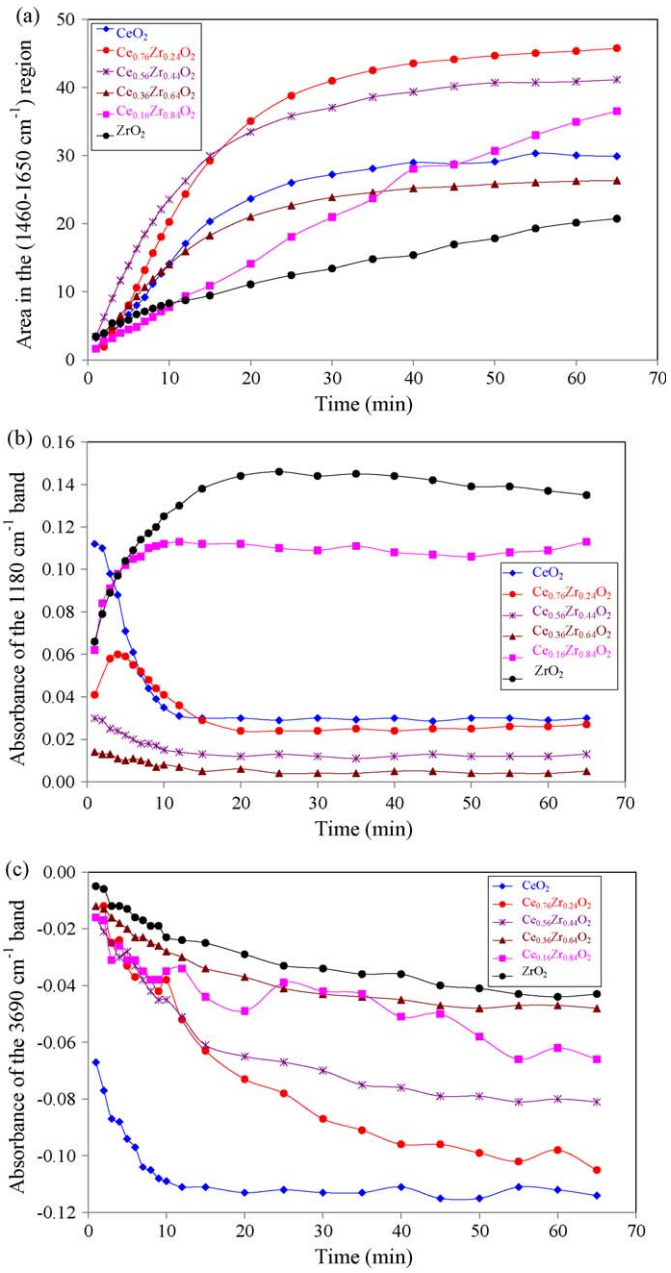

Fig. 8. Evolution of adsorbed intermediates estimated from DRIFTS spectra obtained with $Ce_xZr_{1-x}O_2$-500 catalysts under NO + O_2 at 350 °C: (a) nitrates, (b) nitrites, and (c) hydroxyl groups.

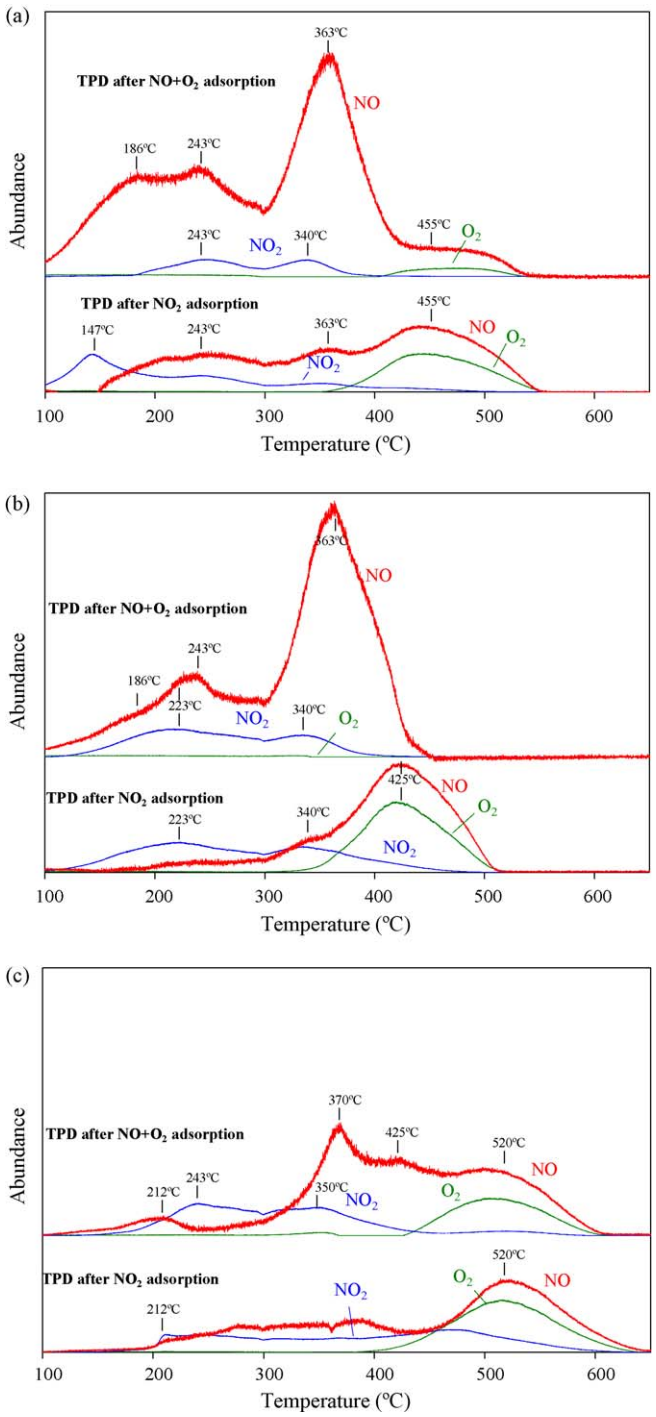

Fig. 9. He-TPD after NO_2 and NO + O_2 adsorption at 60 °C on samples: (a) CeO_2, (b) $Ce_{0.76}Zr_{0.24}O_2$, and (c) ZrO_2.

catalysts active for the oxidation of NO in the presence of O_2 can be also active for the reverse reaction in the absence of O_2, i.e. the dissociation of NO_2 back to NO and $1/2O_2$ [38]. Hence, on catalysts having a low NO oxidation activity, the desorption of NO_2 ad-species should lead mainly to NO_2 as the desorbed product in the gas phase. By contrast, catalysts with high NO oxidation ability and/or strong redox activity may release NO_2 ad-species preferentially as NO if the desorption is carried out under inert atmosphere, which is the case here. For kinetic reasons, NO_2 decomposition is thought to be promoted by the temperature. The situation is further complicated by the possibility for desorbing NO to be re-oxidized back to NO_2 on a reactive oxygen site. This could result in several oxidation/reduction turnovers for the NO and NO_2 molecules depending on their positions where they are emitted within the catalyst bed [38]. Second, the thermodynamics of the NO_2 dissociation reaction predict a progressive displacement of the equilibrium towards the formation of NO and O_2 at medium–high desorption temperatures. In other words, this implies that, even if NO_2 is the primary desorbing species, both a fraction of NO_2 and the complement as the sum NO + $1/2O_2$ would be detected. Once again, the situation is further complicated by the fact that re-adsorption of NO_2 dissociation products (NO and O_2) may push the thermodynamic equilibrium towards their formation, and reversely.

According to the results obtained by DRIFTS, the adsorption of NO + O_2 or NO_2 on ceria-zirconia leads to the formation of nitrites

and nitrates as the major ad-NO_x species, whereas the adsorption of NO in its molecular form is not significant. In general, nitrates are known to have a superior thermostability in comparison with nitrites, which manifest some instability at medium temperatures (Fig. 7). From Fig. 9a–c), it can be stated that the desorption profiles obtained after NO_2 adsorption (bottom profiles) usually end at temperatures higher than those obtained during the desorption of NO + O_2 (top profiles). Considering that NO oxidation is kinetically limited at the adsorption temperature (60 °C), the amount of the most stable ad-NO_x species, i.e. nitrates, is thought to be superior for the NO_2 adsorption in comparison with the adsorption of NO + O_2. Here, this can be easily checked by comparing the bottom and top profiles on Fig. 9a–c above ca 350–400 °C. The decomposition of nitrates should in principle release NO_2 [38] which should be indeed progressively transformed to NO and O_2 when switching to medium–high temperatures due to thermodynamics. This process can be easily visualized in the TPD patterns by the simultaneous evolution of NO + 1/2O_2, with an almost constant ratio between the two peaks, above ca 350–400 °C, i.e. at temperatures corresponding to the tail of the last NO_2 peak (Fig. 9a–c). For a single catalyst, it can be observed that the NO + 1/2O_2 peak is higher for (NO_2)-TPD rather than for (NO + O_2)-TPD. By comparing the NO + 1/2O_2 peaks, this time between the different catalysts, it can be observed that ZrO_2 (NO + 1/2O_2 peak at 520 °C) has the most stable nitrates among the catalysts tested. By contrast, NO_3^- species are considerably less stable for $Ce_{0.76}Zr_{0.24}O_2$ and CeO_2 compositions.

On the other hand, the TPD peaks observed at temperatures inferior to 350 °C (Fig. 9a–c) are mostly related to the desorption of the most instable species, i.e. nitrites and nitro species [35,38,39], but also partly to the desorption of some of their possible decomposition/oxidation products, which again adds some complexity to the analysis of the data. Moreover, the decomposition mechanisms of nitrites and nitrates are not well known because they can yield different products depending on their peculiar bonding mode with the surface and the redox properties of the anchoring cation. By looking at the TPD patterns on Fig. 9a–c, it can be observed that all the catalysts desorb NO, giving one or several broad peaks in the 180–250 °C range and most likely one sharp peak in the 340–380 °C range. In general, the maximum of NO production lags just a few degrees above the maximum of a NO_2 peak, which suggests that some desorbing NO_2 is reduced to NO during the TPD under He. Moreover, when the intensity of the NO_2 peak is relatively high, the intensity of the NO peak is relatively low, and reversely (see (NO + O_2)-TPD on Fig. 9a–c). Strikingly, the catalysts $Ce_{0.76}Zr_{0.24}O_2$ and CeO_2 are characterized by superior NO/NO_2 ratio and TPD peaks occurring at inferior temperatures in comparison with the ZrO_2. These data give indirect information on the ability of the different catalysts to dissociate NO_2. The sequence occurring during the TPD under He is as follows: the nitrites created during the adsorption stage simply desorb as NO_2 around 180–250 °C or decompose on a Ce^{3+}–□ reduced surface site, to give NO and O*, depending on the redox activity of the catalysts. The desorbing NO_x can further react with these O* species to yield a nitrate species and another Ce^{3+}–□ reduced site. Some of the less stable nitrates (or the desorbing NO_2) dissociate on these Ce^{3+}–□ reduced sites from 300 °C and above to release NO. The dissociation may occur with or without O_2 release depending on the oxygen mobility in the catalysts and the temperature. To sum up, the Ce-rich compositions, which are far more active than the Zr-rich ones for the formation of nitrates (see DRIFTS results) and the oxidation of NO in NO + O_2 atmosphere are also more active for the dissociation of NO_2 in absence of O_2. Hence, one can conclude that the oxidation of NO to NO_2 and or nitrites to nitrates is reversible, and the NO_2 yielded by each catalyst under reaction conditions (Fig. 3b) is the net result of these reversible processes.

3.4.2. He-TPD after NO + O_2 adsorption at 350 °C

The desorption of NO_x adsorbed on CeO_2, $Ce_{0.76}Zr_{0.24}O_2$ and ZrO_2 was also studied in a flow reactor after 1-h isothermal NO oxidation tests carried out at 350 °C. These NO oxidation experiments (not shown here) gave results consistent with those presented on Fig. 3b despite different conditions (isothermal instead of ramp experiments, and lower GHSV). Whereas CeO_2 and $Ce_{0.76}Zr_{0.24}O_2$ gave NO_2 conversions close to the maximal conversions predicted by thermodynamics already at 400 °C, the ZrO_2 catalyst lagged well behind, never reaching the maximal conversion values. The TPD profiles obtained after cleaning the catalysts with He at 350 °C for 1 h are compiled in Fig. 10a–c. It has to be noted that O_2 profiles cannot be given here in contrast to Section 3.4.1 due to the quantification method used (FTIR). Before TPD, some of the less stable adsorbed NO_x species may have been removed during the cleaning step (NO_x release due to a change in adsorption equilibrium when switching to O_2-free atmosphere). Thus, only the ad-NO_x species that are stable at 350 °C remain on the surface and are detected during the TPD experiments.

Consistently with the results presented on Fig. 9, the desorption of the ad-NO_x species adsorbed on the different catalysts, most likely nitrates, yield NO_2 first and then NO at higher temperatures

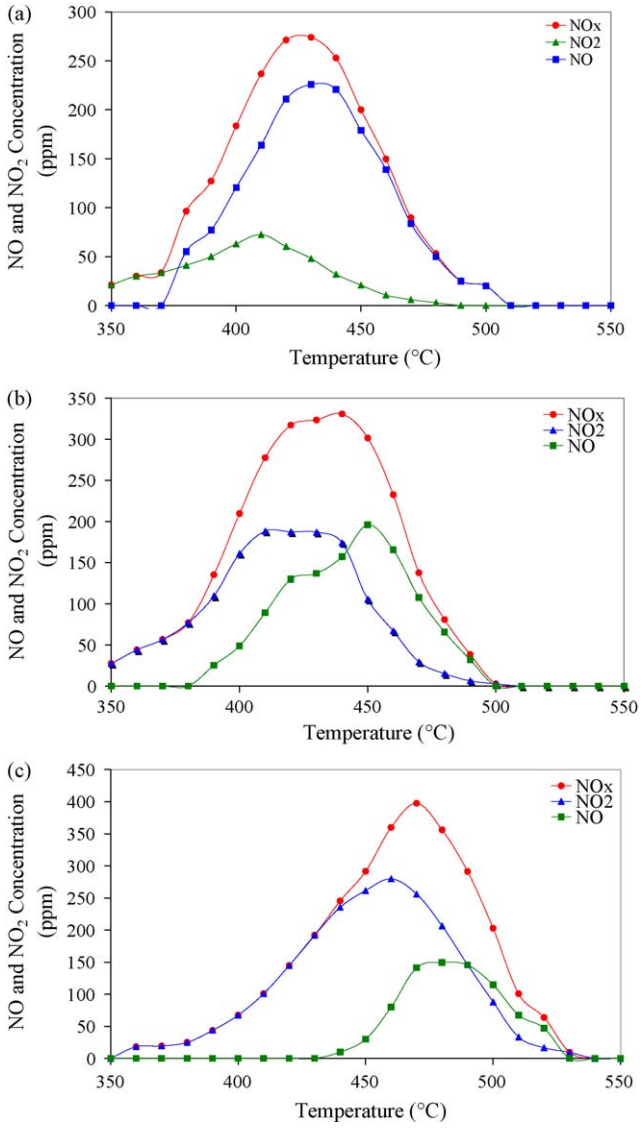

Fig. 10. He-TPD after NO + O_2 adsorption at 350 °C on samples: (a) CeO_2, (b) $Ce_{0.76}Zr_{0.24}O_2$, and (c) ZrO_2.

(Fig. 10). Again, the production of NO arises from the thermodynamic-driven decomposition of nitrogen dioxide and/or NO_2 dissociation on reduced metal sites. The latter process results in a significantly lower production of NO_2 for the Ce-rich compositions in comparison with ZrO_2, despite its relative inefficiency for NO oxidation (Fig. 7). The contrary (higher NO_2 production for the Ce-rich compositions) would have been expected if the TPD were conducted under O_2-containing atmosphere instead of He, because in that case the NO_2 dissociation reaction would not take place significantly due to the lack of reduced sites. Also worth noting is the higher thermostability of the nitrates adsorbed on the ZrO_2 surface. This can be visualized by comparing the amount of the total-NO_x desorbed from the catalysts and/or the end temperatures of the TPD patterns (Fig. 10), which are both significantly increased for ZrO_2. In that respect, note that the BET surface areas of the three catalysts selected are quite similar to each other (64–67 m^2/g), which facilitates the comparison. Therefore, the trends observed in the flow-reactor experiments are consistent with those exposed in Section 3.4.1. Now, the question arises whether the nitrates have an inhibiting or promoting effect on NO oxidation, i.e. the NO_2 released from the catalyst. In the literature, the kinetics of NO oxidation were described adequately using both a Langmuir–Hinshelwood and an Eley–Rideal mechanism (namely on Pt-based catalysts), which makes that the "real" NO oxidation mechanism is not known in detail [38]. On the one hand, nitrates could be considered as intermediates in the production for NO_2, because nitrogen dioxide is expected to be released from their decomposition under O_2-containing atmosphere. On the other hand, nitrates could also be considered as inhibitors because they may occupy some sites involved in the NO oxidation reaction. In fact, NO oxidation requires an O^* active oxygen, which may also be needed for the production of nitrates, at least when they are formed via nitrite oxidation. This may enter in the kinetic limitations relevant to the NO oxidation at low–medium temperatures and a coverage-dependence on NO oxidation rate is expected. From the present data, it is clear that the adsorption equilibrium, or in other words the stability of the nitrates, depends both on the temperature, the atmosphere and the redox activity of the site and/or catalyst. ZrO_2 does not yield NO_2 at 350 °C in blank experiments (Fig. 3b) while $Ce_{0.76}Zr_{0.24}O_2$ and CeO_2 does. Thus, these results demonstrate that the production of NO_2 in the range of temperatures relevant to soot oxidation not only depends on the NO/nitrites oxidation capacity of the catalyst used but also on the adsorption strength of the nitrates in NO oxidation conditions. It is interesting that the NO and NO_2 desorption profiles obtained with CeO_2 and $Ce_{0.76}Zr_{0.24}O_2$ (Fig. 7a and b, respectively) are different. $Ce_{0.76}Zr_{0.24}O_2$ yields similar amount of NO and NO_2 while CeO_2 yields a much lower amount of NO_2. This can be attributed to the stabilizing effect of zirconium on the nitrate species, that is, part of the nitrates formed upon NO/nitrites oxidation on the CeO_2 catalyst release during the cleaning step while they remain on the catalyst in the case of $Ce_{0.76}Zr_{0.24}O_2$. However, the NO_2 production capacity of CeO_2 and $Ce_{0.76}Zr_{0.24}O_2$ are equal, as observed in Fig. 3b. This could indicate that zirconium plays a double role in the NO_2 formation mechanism catalyzed by $Ce_{0.76}Zr_{0.24}O_2$. On one hand, zirconium stabilizes the nitrates formed upon NO/nitrites oxidation, as mentioned. On the other hand, Zr improves the oxidation capacity of ceria [21,39,40], as was confirmed by the *in situ* DRIFTS experiments discussed in the previous section. The net result on NO_2 production of both opposite effects is that CeO_2 and $Ce_{0.76}Zr_{0.24}O_2$ behave equal.

4. Conclusions

In this study, $Ce_xZr_{1-x}O_2$ (x from 0 to 1) catalysts prepared by co-precipitation have been characterized and tested for soot combustion by NO_x/O_2, paying special attention to the adsorption/desorption mechanisms of NO_x on the different catalysts and to the effect of these steps on the soot oxidation pathways. The following conclusions can be summarized.

CeO_2 and $Ce_{0.76}Zr_{0.24}O_2$ present superior activity for soot oxidation with NO_x/O_2 than catalysts with higher amount of Zr, and the catalytic activity for soot combustion of cerium-containing catalysts depends on their NO_2 production capacity. A linear relationship between the temperature of maximum NO_2 production ($T_{max}NO_2$) and the temperature of half soot conversion (T50%) has been obtained.

For ceria-zirconia mixed oxides, the catalytic activity for NO oxidation to NO_2 depends on their composition rather than on the BET area.

As deduced from DRIFTS data, nitrites and nitrates in chelated or bridged configurations represent the main ad-NO_x species formed upon adsorption of NO_x on $Ce_xZr_{1-x}O_2$ in the 30–350 °C range both in presence/absence of O_2. The possible routes leading to the formation of the different ad-NO_x species have been investigated in detail. All the $Ce_xZr_{1-x}O_2$ compositions have OH groups with oxidizing properties, which can react with NO to give preferentially nitrites, and possibly nitrates. The main pathway leading to nitrates is however the surface oxidation of nitrites (which can also form via NO oxidation and NO_2 sorption) by activated O^* species. For a given catalyst, parameters promoting the formation of nitrates (and NO_2 via NO oxidation) are namely the temperature and the ability of the catalyst structure to take advantage of the presence of O_2 in the gas phase. Among the $Ce_xZr_{1-x}O_2$ series, the compositions with x = 0.76 and 0.56 have the most rapid kinetics of nitrates production at 350 °C, while ZrO_2 has the lowest one.

The rate of the catalyzed oxidation of NO to NO_2 in the temperature range relevant to soot oxidation follows roughly the same trend observed for the production of nitrates but is also affected by the adsorption strength of the latter. Hence, Zr-rich catalysts contain strong NO_x adsorption sites, and require higher temperatures than the Ce-rich ones to transform nitrites into nitrates via surface oxidation, which explains their poor catalytic activity for NO_2 production in comparison to cerium-rich formulations.

The oxidation of NO to NO_2 and/or nitrites to nitrates over the catalysts studied is reversible, and the NO_2 yielded by each catalyst under reaction conditions is the net result of these reversible processes.

Acknowledgement

The authors gratefully acknowledge the Spanish Ministry of Education and Science for the financial support (Project MAT2006-12635).

References

[1] J.P.A. Neeft, M. Makkee, J.A. Moulijn, Fuel Process. Technol. 47 (1996) 1–69.
[2] B.R. Stanmore, J.F. Brilhac, P. Gilot, Carbon 39 (2001) 2247–2268.
[3] B.A.A.L. van Setten, M. Makkee, J.A. Moulijn, Catal. Rev. – Sci. Eng. 43 (2001) 489–564.
[4] M.V. Twigg, Appl. Catal., B 70 (2007) 2–15.
[5] P. Fornasiero, T. Montini, M. Graziani, S. Zilio, M. Succi, Catal. Today 137 (2008) 475–482.
[6] A. Bueno-López, K. Krishna, M. Makkee, J.A. Moulijn, J. Catal. 230 (2005) 237–248.
[7] B. Azambre, S. Collura, J.V. Weber, Appl. Surf. Sci. 253 (2006) 2296–2303.
[8] A. Setiabudi, M. Makkee, J.A. Moulijn, Appl. Catal., B 50 (2004) 185–194.
[9] I. Atribak, I. Such-Basáñez, A. Bueno-López, A. García-García, J. Catal. 250 (2007) 75–84.
[10] E. Aneggi, C. de Leitenburg, G. Dolcetti, A. Trovarelli, Catal. Today 114 (2006) 40–47.
[11] I. Atribak, A. Bueno-López, A. García-García, Catal. Commun. 9 (2008) 250–255.
[12] I. Atribak, A. Bueno-López, A. García-García, J. Catal. 259 (2008) 123–132.

[13] K. Krishna, A. Bueno-López, M. Makkee, J.A. Moulijn, Appl. Catal., B 75 (2007) 189–200.
[14] K. Krishna, A. Bueno-López, M. Makkee, J.A. Moulijn, Appl. Catal., B 75 (2007) 201–209.
[15] K. Krishna, A. Bueno-López, M. Makkee, J.A. Moulijn, Appl. Catal., B 75 (2007) 210–220.
[16] N. Miyakawa, H. Sato, H. Maeno, H. Takahashi, JSAE Rev. 24 (2003) 269.
[17] D. Michel, M. Perez, Y. Jorba, R. Collonges, J. Raman Spectrosc. 5 (1976) 163–180.
[18] P. Fornasiero, G. Balducci, R. di Monte, J. Kaspar, V. Sergo, G. Gubitosa, A. Ferrero, M. Graziani, J. Catal. 164 (1996) 173–183.
[19] J. Kašpar, P. Fornasiero, G. Balducci, R. Di Monte, N. Hickey, V. Sergo, Inorg. Chim. Acta 349 (2003) 217–226.
[20] H. Vidal, J. Kašpar, M. Pijolat, G. Colon, S. Bernal, A. Cordón, V. Perrichon, F. Fally, Appl. Catal., B 27 (2000) 49–63.
[21] J.I. Gutiérrez-Ortiz, B. de Rivas, R. López-Fonseca, J.R. González-Velasco, Appl. Catal., B 65 (2006) 191–200.
[22] M. Yashima, K. Morimoto, N. Ishizawa, M. Yoshimura, J. Am. Ceram. Soc. 76 (1993) 1745–1750.
[23] M. Yashima, K. Morimoto, N. Ishizawa, M. Yoshimura, J. Am. Ceram. Soc. 76 (1993) 2865–2868.
[24] M. Yashima, H. Arashi, M. Kakihana, M. Yoshimura, J. Am. Ceram. Soc. 77 (1994) 1067–1071.
[25] P. Fornasiero, A. Speghini, R. Di Monte, M. Bettinelli, J. Kašpar, A. Bigotto, V. Sergo, M. Graziani, Chem. Mater. 16 (2004) 1938–1944.
[26] D. Terribile, A. Trovarelli, J. Llorca, C. de Leitenburg, G. Dolcetti, Catal. Today 43 (1998) 79–88.
[27] M. Adamowska, S. Muller, P. Da Costa, A. Krzton, P. Burg, Appl. Catal., B 74 (2007) 278–289.
[28] F.E. López-Suárez, A. Bueno-López, M.J. Illán-Gómez, Appl. Catal., B 84 (2008) 651–658.
[29] A. Bueno-López, K. Krishna, M. Makkee, J.A. Moulijn, Catal. Lett. 99 (2005) 203–205.
[30] L. Zenboury. PhD thesis, Paul Verlaine University, 2009.
[31] E. Mamontov, R. Brezny, M. Koranne, T. Egami, J. Phys. Chem. B 107 (2003) 13007–13014.
[32] C. Descorme, Y. Madier, D. Duprez, J. Catal. 196 (2000) 167–173.
[33] B. Azambre, L. Zenboury, F. Delacroix, J.V. Weber, Catal. Today 137 (2008) 278–282.
[34] K.I. Hadjiivanov, Catal. Rev. – Sci. Eng. 42 (2000) 71–144.
[35] A. Martínez-Arias, J. Soria, J.C. Conesa, X.L. Seoane, A. Alcoraya, R. Cataluña, J. Chem. Soc., Faraday Trans. 91 (1995) 1679–1687.
[36] B. Gil, K. Mierzyńska, M. Szczerbińska, J. Datka, Appl. Catal., A 319 (2007) 64–71.
[37] V.V. Pushkarev, V.I. Kovalchuk, J.L. d'Itri, J. Phys. Chem. B 108 (2004) 5341–5348.
[38] W.S. Epling, L.E. Campbell, A. Yezerets, N.W. Currier, J.E. Parks, Catal. Rev. – Sci. Eng. 46 (2004) 163–245.
[39] G. Balducci, J. Kašpar, P. Fornasiero, M. Graziani, M.S. Islam, J.D. Gale, J. Phys. Chem. B 101 (1997) 1750–1753.
[40] G. Balducci, J. Kašpar, P. Fornasiero, M. Graziani, M.S. Islam, J. Phys. Chem. B 102 (1998) 557–561.